Neutral beam heating of a RFP plasma in MST

J. Waksman, J. K. Anderson, M. D. Nornberg, E. Parke, J. A. Reusch et al.

Additional information on Phys. Plasmas

Neutral beam heating of a RFP plasma in MST

J. Waksman,[1] J. K. Anderson,[1] M. D. Nornberg,[1] E. Parke,[1] J. A. Reusch,[1] D. Liu,[2]
G. Fiksel,[3] V. I. Davydenko,[4] A. A. Ivanov,[4] N. Stupishin,[4] P. P. Deichuli,[4] and H. Sakakita[5]

[1]*Department of Physics, University of Wisconsin-Madison, 1150 University Avenue, Madison, Wisconsin
53706-1390, USA*
[2]*Department of Physics and Astronomy, University of California, Irvine, California 92697-4575, USA*
[3]*Laboratory for Laser Energetics, University of Rochester, 250 E. River Rd, Rochester,
New York 14623-1299, USA*
[4]*Budker Institute of Nuclear Physics, 11, Akademika Lavrentieva Prospect, Novosibirsk 630090, Russia*
[5]*National Institute of Advanced Industrial Science and Technology (AIST), 1-1-1 Umezono, Tsukuba,
Ibaraki 305-8568, Japan*

Electron temperature is observed to rise due to neutral beam injection (NBI) in the Madison Symmetric Torus (MST). Heating is observed to be 100 ± 50 eV in the core of 200 kA plasmas. This is the first definitive measurement of auxiliary heating of a reversed-field pinch (RFP). This heating is consistent with a 1D classical model which was developed. This 1D model calculates the evolving thermal conductivity and ohmic power input profiles during enhanced confinement, and can calculate NBI deposition and classical fast ion diffusion and slowing. The predicted temperature change is consistent with measured beam heating both during and after enhanced confinement, which is consistent with previous observations that fast ions are well confined and behave roughly classically in the RFP. © *2012 American Institute of Physics.*
[http://dx.doi.org/10.1063/1.4772763]

I. INTRODUCTION

A high-power neutral beam injector (NBI) can serve several important scientific purposes on a reversed field pinch (RFP) device. The injected fast ions can provide momentum and current drive, and can provide information on fast particle dynamics. In addition, auxiliary heating may help probe the beta limit of RFP plasmas.[1]

The NBI has been well-studied on tokamaks, where the auxiliary heating it provides is necessary because ohmic heating alone is insufficient to reach the energies needed for fusion.[2–4] The NBI has become a dominant source of auxiliary heating for tokamak plasmas.[5,6] A minimum of 33 MW of NBI power is being planned for ITER[7] to help it achieve the necessary high temperatures for significant fusion energy.

The NBI is not as well-studied on the RFP, which can reach ignition with ohmic heating alone provided that transport and impurity losses are sufficiently small.[8] Werley[9] calculated that ignition could be reached with Ohmic heating alone at a plasma current as low as 8.1 MA, though the possibility exists that auxiliary heating may play an important role in future RFPs.

In addition, the NBI will not heat as efficiently on the RFP as it does on the tokamak. This is primarily because energy confinement times of background ions and electrons in standard RFPs are poor relative to tokamak plasmas[10] (in the Madison Symmetric Torus (MST), the standard energy confinement time of electrons is ≈ 1 ms). In fact, there has been no prior conclusive evidence of auxiliary heating of a RFP from any source of auxiliary power.

Auxiliary heating through NBI was explored in TPE-RX.[11] Powerful NBI (nominally 1.2 MW) injected radially into high density enhanced-confinement plasmas showed an increase in soft X-ray signal consistent with approximately 30 eV ($\frac{\Delta T_e}{T_e} \approx 0.05$), as well as an increase in plasma current.[12] However, this heating was within the measurement uncertainty and could not be confirmed with Thomson scattering.

While fast ion confinement is long (>20 ms) relative to plasma confinement times in MST,[13] the fact that the standard MST energy confinement time is small relative to the fast ion slowing down time ($\tau_\varepsilon^{i,e} \ll \tau_{slow}^{fi}$) makes NBI heating difficult to achieve.

This paper demonstrates that auxiliary electron heating of around 100 eV in the MST plasma core due to NBI has been achieved and confirmed by Thomson scattering. The temporal evolution and profile of the induced heating are understood by a simple, classical 1D heat balance.

II. EXPERIMENTAL SETUP

The MST is a reversed field pinch with minor radius $a = 0.52$ m and major radius $R = 1.5$ m. A 1 MW NBI has been installed (Fig. 1) that fires neutrals with an energy of approximately $E_{fi} = 25$ keV and a current of up to $I_{fi} = 40$ A. The NBI can be fired at full power for 20 ms, though a shorter pulse was used for in this work (see Fig. 2). The NBI fuel in this study is approximately 97% hydrogen and 3% deuterium. The deuterium produces the measured neutron flux, which can be used to calculate fast ion confinement. A shine-thru detector measures the amount of beam power that passes through the plasma without being deposited.

In order to maximize NBI heating, the beam was fired into enhanced confinement (PPCD) plasmas. PPCD plasmas demonstrate a reduction of magnetic field fluctuations, an
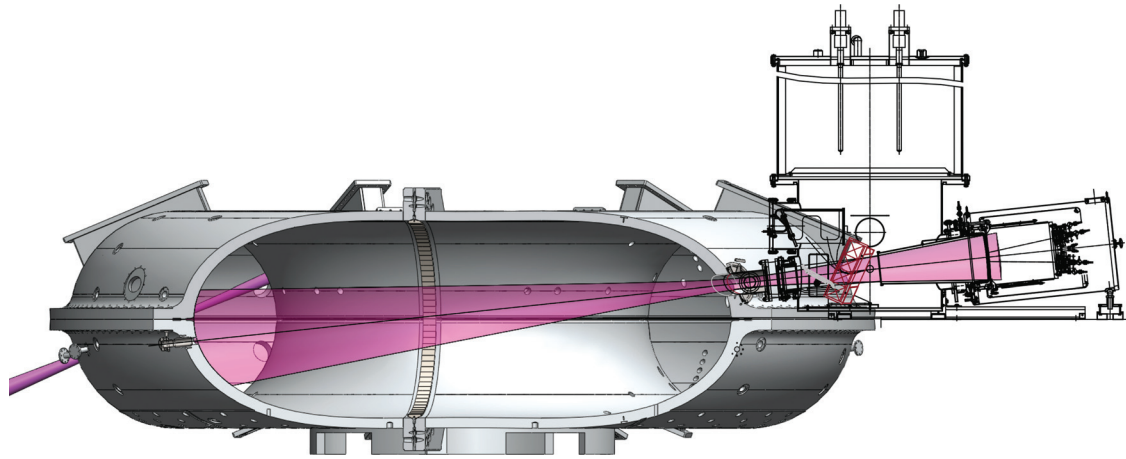
19, 122505-1

FIG. 1. Scale drawing of MST, the NBI, and the neutral beam path.

increase in plasma β, and an increase of energy and particle confinement times.[14,15] Conventional MST PPCD plasmas ($I_P \approx 400\,\text{kA}, n_e \approx 1 \times 10^{13}\,\text{cm}^{-3}$) see approximately a 50% decrease in magnetic fluctuation amplitudes, a 50% increase in poloidal beta, and a five-fold increase in energy confinement times.[16] The increased energy confinement times allow energy deposited by the NBI to stay in the plasma long enough for measurable temperature increases.

Key diagnostics in this study characterize the evolution of the kinetic profiles. Electron density profiles were measured with a multichannel far-infrared-interferometer system (FIR) that has 11 channels and a time response of $1\,\mu\text{s}$.[17] Electron temperature profiles were measured with a high

time resolution ($\sim$1 kHz) Thomson scattering system[18] at 22 radial locations and at 30 time points. To reduce statistical noise in the data, an ensemble of similar discharges was assembled, judged by magnetic activity, plasma current, and plasma density (Fig. 2). The final ensemble was made with 22 "NBI On" shots and 22 "NBI Off" shots. Thomson temperature data are plotted in Fig. 3. In this case, "Core Te" is the statistical mean of the five innermost radial Thomson measurements (r/a < 0.11), which is where heating is strongest. ΔTe, which is the difference of T_e between the "NBI On" and "NBI Off" cases, is investigated in detail in Sec. V.

The rapid increase in electron temperature and stored energy in the plasma core even without NBI is caused by reduced transport due to the reduction in magnetic fluctuations during PPCD. Thermal conductivity in MST is extremely sensitive to mid-radius magnetic mode activity, but not at all sensitive to core magnetic mode activity.[19] In Fig. 2, it can be seen that suppression of the mid-radius magnetic fluctuations (m = 1, n = 7–12) is the same in both the NBI On and NBI Off cases. Most of the electron temperature increase during PPCD (Fig. 3) is due to the suppression of the mid-radius modes, but additional heating due to NBI should be described through classical slowing down of beam ions on a thermal background.
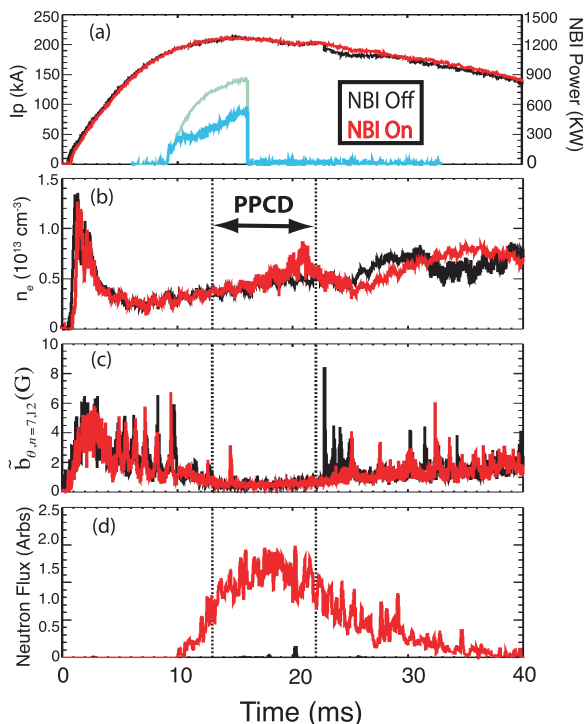

FIG. 2. Data from an example "NBI On" shot and an example "NBI Off" shot. Plasma current is plotted in (a), line-averaged electron density in (b), mid-radius magnetic fluctuations in (c), and neutron flux in (d). In addition, NBI power is plotted in (a). Input NBI power is green and absorbed NBI power (NBI power minus shine-thru) is blue.
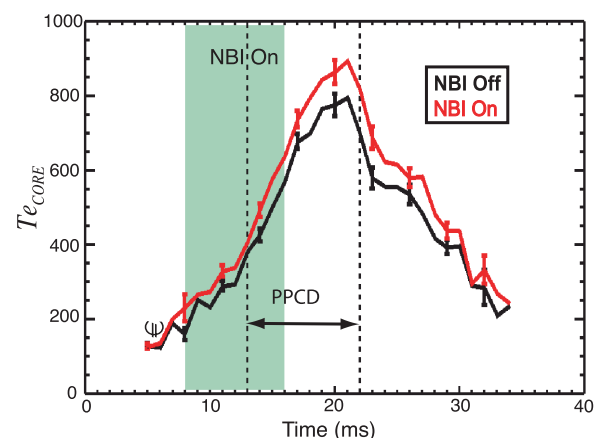

FIG. 3. Thomson scattering measurement of core (r/a < 0.11) electron temperature for the "NBI On" and "NBI Off" 200 kA PPCD plasma ensembles.

It should be noted that uncertainty in the measurement of electron temperature makes it difficult to see the beam heating in Fig. 3. Some data points, such as a low NBI Off data point at 8 ms, show small random fluctuations that do not represent NBI heating. The amount of heating in the NBI On case can be seen more clearly in Fig. 6.

III. MODELING TEMPERATURE EVOLUTION IN MST

Temperature evolution in MST is studied with a simple heat balance model. In this model, heat diffusion coefficients (χ_e) are determined from the calculated net conducted power in the NBI Off case, solved for concentric circular volume elements. These same χ_e profiles are used for the NBI On case, and are used to solve a differential equation for the time evolution of the electron temperature profile. Beam heating deposition is modeled four different ways, and each resulting temperature profile is compared to the data.

A key assumption in this analysis is holding the fixed χ_e profiles determined in the non-NBI discharges for the NBI-heated discharges. The justification lies in the measured magnetic mode amplitudes: the mid-radius, observed to correlate with core electron temperature,[19] is not altered during NBI operation.

The stored energy balance for electrons in a finite volume is

$$\dot{W}_e = \frac{\partial}{\partial t}\int \frac{3}{2} n_e T_e dV = P_\Omega + P_B - P_{ei} + A\chi_e n_e \nabla T_e, \quad (1)$$

where

$$P_{ei} = \int v_\varepsilon^{ei} n_e (T_e - T_i) dV. \quad (2)$$

In Eq. (1), P_Ω (ohmic power), P_B (beam power), and P_{ei} (electron-ion power exchange via Coulomb collisions) are volume-integrated. A is the surface area of the volume element. In addition, a sign convention has been adopted with positive χ_e for negative ∇T_e. In the case of electrons in MST, high ohmic power (0.5–10 MW) is mostly balanced out by large thermal diffusion ($\chi_e \approx 10 - 100 \, \text{m}^2/\text{s}$). Radiative and convective losses have been dropped from this equation. Convective energy losses have been calculated to be less than 10% of conductive energy losses in MST,[20] and radiative losses are very small relative to ohmic input power for r/a < 0.9.[21]

Equation (1) is solved for the χ_e profiles using calculated P_Ω profiles for the NBI Off case. In order to investigate the effect of NBI deposited power onto the electrons, Eq. (1) is re-cast onto a set of concentric circular volume elements. Because ohmic power and conducted heat are dominant, a heat conduction parameter X_Q is defined

$$Q_c(i) = \chi_e(i)n_e(i)\nabla T_e(i)A(i), \quad (3)$$

$$X_Q(i) = \frac{Q_c(i-1) - Q_c(i)}{\nabla T_e(i)}. \quad (4)$$

Here, $X_Q(i)\nabla T_e(i)$ is the net heat conducted into the *ith* circular volume element. In defining heat conduction in this manner, we find improved numerical stability.

Because density changes slowly relative to temperature during these enhanced confinement periods (see Fig. 2), Eq. (1) can be re-written for each volume element

$$\frac{\partial T_e}{\partial t} = \frac{P_\Omega + P_B - (v_\varepsilon^{ei}N_e)(T_e - T_i) + X_Q\nabla T_e}{1.5N_e}, \quad (5)$$

where N_e is the total number of electrons within the volume slice. Equation (5) can be written for each discrete volume element.

Electron-to-ion heat transfer is included in the power balance, but is not a significant factor for electrons. Several models of ion temperature profiles showed a negligible impact on the T_e model. Even forcing $T_i = 0$ at all locations and times did not significantly impact the resultant T_e profile. For this simulation, it was assumed that ion temperature profiles were initially the same as the electron temperature, but did not rise without auxiliary heating during the PPCD period, which is consistent with previous measured results in MST.[15]

A heat conduction partial differential equation with both spatial and time dependence, such as Eq. (5), can be solved implicitly using the Crank-Nicolson method for numerical evaluation of solutions of partial differential equations.[22] Solving the equation in this way forces the NBI Off case to match the NBI Off data, as can be seen in Fig. 5, where the green solid line is the solution of Eq. (5) with the NBI Off electron temperature profile as the initial condition. This solution technique is repeated to model NBI heated discharges. Several methods of calculating P_B are discussed in Sec. IV.

IV. MODELING BEAM HEATING IN MST

Beam deposition and fast ion heating are modeled four different ways in this paper. The first method uses the TRANSP/NUBEAM code that was developed at PPPL for tokamaks.[23,24] The second method is a 1D classical fast ion model that was developed specifically for this research (hereafter called the "1D heating + deposition model"), and includes both classical slowing down and classical diffusion. The other two methods are hybrid models.

While TRANSP and NUBEAM are powerful codes for tokamaks, they use a toroidal-flux-based radial coordinate, which is not monotonic in the RFP (and there is particularly large toroidal field reversal in PPCD plasmas). TRANSP can only model a RFP by ignoring the portion of the plasma beyond the reversal surface (which truncates these discharges at r/a ≈ 0.65). In addition, the TRANSP runs used here are restricted to a fixed equilibrium and kinetic profile, used mainly to model the build-up of fast ion density. TRANSP/NUBEAM produces a model of the beam heat deposition profile for electrons and ions, which is input to Eq. (5).

The 1D heating + deposition model was developed to calculate both fast ion deposition and dynamics in a RFP.

Determining the birth locations of the fast ions is a two step process. An array of fast neutral "beamlets" is defined that follows the MST NBI beam path. The distribution of fast neutrals across each beamlet is described by a half-width of 5 cm, and they spread out inside the plasma at an angle of 3.35° (both numbers are calculated from the NBI geometry).

Ion deposition is computed using tabulated ionization cross sections[25] at each point in space along each beamlet's path. These deposited fast ions are distributed evenly over the radial locations in their initial gyro-orbit. These fast ions are then grouped into a set of fast ion "beamlets" that are localized in radius (r) and indexed by the time at which they were born (t'). Each fast ion beamlet is born with an energy ($E_f(r,t')$) equal to the full NBI energy (25 kV) and with a number of fast ions ($N_f(r,t')$) dictated by the beam ionization calculations. The beam is assumed to have a 3 ms ramp-up phase before reaching a plateau of 40 A of current, matching the experimental waveform. The total number of fast ions born at any given time must be a function of the beam current and shine-thru

$$\sum_{r=0}^{r=r_{max}} N_f(r,t') = I_{BEAM}(t')\Delta t(1 - shinethru(t'))/q_f. \quad (6)$$

In Eq. (6), Δt is the length of the code time step and q_f is the fast ion charge. These fast ions are then allowed to diffuse classically with a particle flux in the form of Fick's diffusion law

$$\Gamma_\perp = -D_\perp \nabla_\perp n_f, \quad (7)$$

$$D_\perp = \sum_{s'} v_\perp^{f/s'} r_{Larmor}^2 \frac{(Te+Ti)}{2Te}. \quad (8)$$

For typical MST conditions, $D_\perp \approx 1\,\mathrm{m^2/s}$. It is assumed that there are no charge exchange losses and that slowing down is classical. This assumption is justified because charge exchange losses are reduced during PPCD due to lower neutral densities, particularly in the plasma core. Fast ion dynamics dominated by classical slowing down is consistent with Fiksel *et al.*[14] It is also assumed that there are no prompt ion losses, due to the direction and relatively large magnitude of the magnetic field near the wall. This is a small deviation from previous calculations which found prompt ion losses of $\approx 10\%$ in co-current tangential 20 kV deuterium NBI in MST.[26]

These fast ions will then lose energy through classical collisions to both background ions and electrons. The energy lost by a beamlet with energy E_f in a time Δt is

$$\Delta E_f = \sum_s E_f(1 - e^{-\Delta t v_\varepsilon^{f/s}}), \quad (9)$$

where the energy loss collision frequency is

$$v_\varepsilon^{f/s} = 2v_0^{f/s}\left[\frac{m_f}{m_s}\Psi\left(\frac{v_f^2}{v_s^2}\right) - \dot\Psi\left(\frac{v_f^2}{v_s^2}\right)\right], \quad (10)$$

where $\Psi(x)$ is the Maxwell Integral $\left(\Psi(x) = \frac{2}{\sqrt\pi}\int_0^x dz\sqrt{z}e^{-z}\right)$. The beam heating at a given radius r at time t is the sum over

the contributions from all beamlets at that radial location. The beamlets created earlier in time will have slowed by a greater amount and will have lost more particles to diffusion than beamlets created later in time. This relationship can be described as

$$P_{B\to s}(r,t) = \sum_{t'=t'(0)}^{t'(t)} \frac{N_f(r,t,t')E_f(r,t,t')\left(1-e^{-\Delta t v_\varepsilon^{f/s}(r,t,t')}\right)}{\Delta t}. \quad (11)$$

These values for P_B can then be used in Eq. (5) to solve for the temperature profiles as a function of time.

The hybrid models involve a combination of the 1D heating + deposition model and the TRANSP/NUBEAM model. In both cases, TRANSP/NUBEAM is used to calculate the fast ion deposition while the 1D heating + deposition model beamlet approach is used to track the fast ions and the resulting heat deposition profile. The difference between the two hybrid models is that one includes classical fast ion diffusion while the other does not.

The different calculated profiles of beam heating on electrons at 22 ms are plotted in Fig. 4. The time point of 22 ms is chosen because it is the average time at which PPCD ended in these pulses (in some shots, the enhanced confinement period ended as early as 21 ms, which is why T_e actually peaks at that point in Fig. 3). The comparison is done further from the end of the NBI pulse in order to see clearly the impact of diffusion on both the data and the code predictions.

In Fig. 4, the TRANSP/NUBEAM model is plotted in brown, the 1D heating + deposition model is plotted in red, and the hybrid models are plotted in blue and orange. The TRANSP/NUBEAM model shows an extremely sharp heating profile, with almost no heating beyond 20 cm. The total volume integrated heat deposited for the hybrid models and the 1D heating + deposition model is within 20% of the TRANSP/NUBEAM model. Note that adding diffusion to the hybrid model flattens out the heating profile, and adds heating out near the edge at a level very similar to the 1D
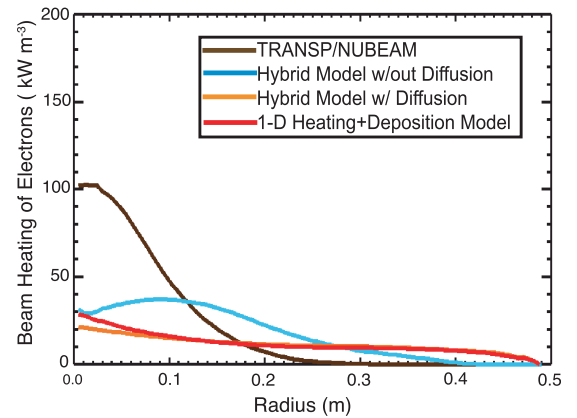

FIG. 4. NBI heating of electrons at t = 22 ms. The brown line is the TRANSP/NUBEAM output, which is sharply peaked in the core. The red line is the 1D heating + deposition model. The blue line is the hybrid model without fast ion diffusion while the orange line is the hybrid model with diffusion.
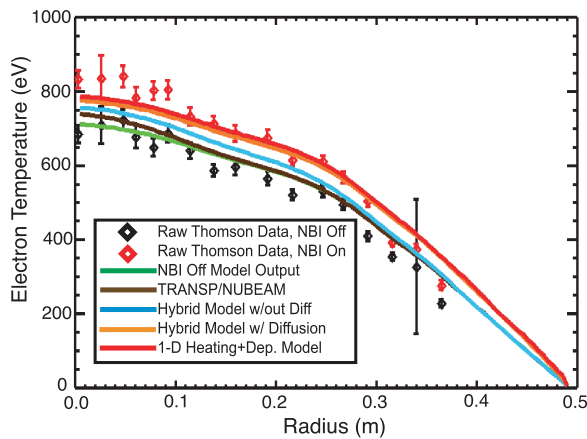
FIG. 5. The MST temperature profile at t = 22 ms. The diamonds with error bars represent the raw Thomson data (black = NBI Off, red = NBI On). The green solid line represents the output of the 1D heating model for the NBI Off case, which matches the raw Thomson data well. The other solid lines represent the output for the four fast ion models, with the same color-coding as Fig. 4.

heating + deposition model, which also includes fast ion diffusion.

V. MODEL RESULTS

The predicted electron temperature profile for each model is plotted at the $t = 22$ ms time slice in Fig. 5. The raw Thomson data are also plotted as black (NBI Off) and red (NBI On) diamonds, with error bars. The output for the NBI Off case is plotted in green, which matches the NBI Off data, as expected. The TRANSP/NUBEAM model shows only core-localized heating, which is consistent with the peaked electron heating profile. The hybrid model without diffusion also shows heating that is core-localized. Its heating profile is not as peaked as the pure TRANSP model, but without particle diffusion most of the fast ions are trapped in the core. The data, however, show significant heating out beyond $r/a = 0.5$. The 1D heating + deposition model and the hybrid model with diffusion are both consistent with this measurement.

The core beam heating (subtracting the NBI Off temperatures from NBI On) is plotted versus time in Fig. 6. The
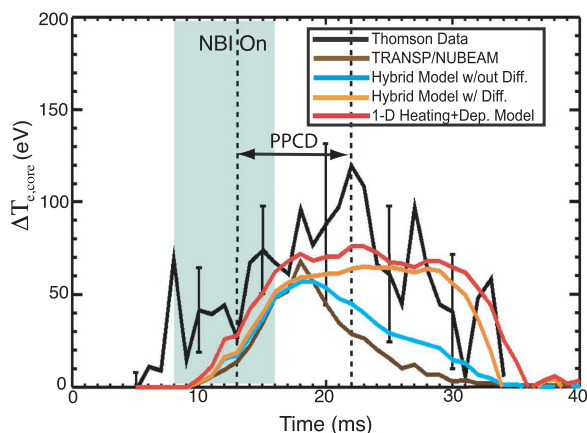

FIG. 6. A plot of core heating ("NBI On"–"NBI Off"). The black solid line with error bars is the raw Thomson data. The other four solid lines are the output for the four different fast ion models, with the same color-coding as Figs. 4 and 5.
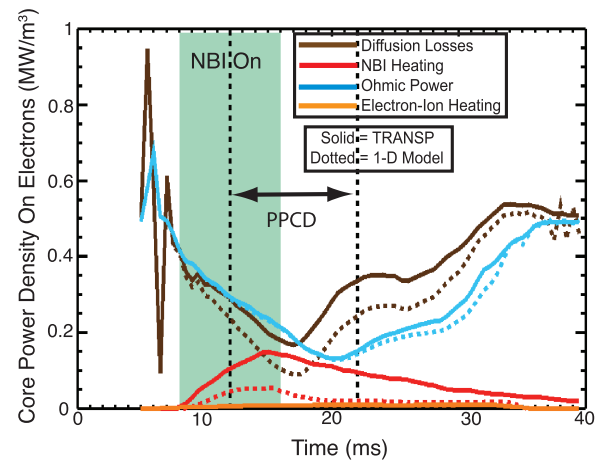

FIG. 7. A plot of power density components on core ($r/a < 0.1$) electrons versus time. The solid lines represent the TRANSP/NUBEAM model while the dotted lines represent the 1D heating + deposition model.

solid black line with error bars is the Thomson data. The other four colored lines are the four fast ion models. These results show that the TRANSP/NUBEAM and no-diffusion hybrid models are consistent with the raw data while the NBI is firing, but they drop off very quickly thereafter. The 1D heating + deposition model and the hybrid model with diffusion stay consistent throughout the length of the simulation.

Measured ΔT_e returns to zero over approximately 10 ms after the end of PPCD, which is consistent with the expected energy confinement and fast ion slowing down time scales.

Increasing the temperature in the core of the plasma requires not only just depositing heat but also confining that heat. The very peaked heating profile of the TRANSP/NUBEAM and diffusion-less hybrid models tends to create a more-peaked temperature profile, which leads to higher $\chi_e \nabla T_e$ (heat conduction). This can be seen in Fig. 7, where the power density components on core electrons are plotted versus time for the TRANSP/NUBEAM model and the 1D heating + deposition model.

The flatter temperature profile in the 1D heating + deposition model leads to substantially lower heat diffusion losses, particularly after the end of PPCD. This is why there is a greater T_e after PPCD in the 1D heating + deposition model, despite the fact that the NBI heating component locally is smaller than in the TRANSP/NUBEAM model (also seen in Fig. 4).

The hybrid model with diffusion, like the 1D heating + deposition model, has a flat NBI heating profile relative to TRANSP/NUBEAM and the hybrid model without diffusion. The fact that heat conduction dominates means that these two models have a greater core ΔT_e, despite less NBI energy deposition in the core than the TRANSP/NUBEAM model and the hybrid model without diffusion. The suppression of the heat diffusion more than compensates for the flatter energy deposition profile.

VI. CONCLUSIONS

Core auxiliary electron heating of approximately 100 eV from short-pulse neutral beam injection has been measured

in a RFP plasma in MST. This heating extends out to approximately half of the plasma minor radius, both during the enhanced confinement period and until approximately 10 ms after the end of this period. This heating is well understood both temporally and spatially with a simple 1D classical model.

Four different fast ion models were used to try to understand the data. A 1D heating + deposition model was created which calculated both beam deposition and fast ion diffusion, a tokamak code (TRANSP/NUBEAM) was used, and two hybrid models were used as well (one with fast ion diffusion, and one without). The TRANSP/NUBEAM model and the diffusion-less hybrid model calculated a core-peaked heating profile, while the other two models calculated a very flat heating profile nearly all the way to the edge of the plasma.

The 1D heating + deposition model and the hybrid model with diffusion were both consistent with the data, even after the end of the enhanced confinement period.

The effect of classical fast ion radial diffusion is to flatten the heat deposition profiles. This avoids a steepening of the T_e profiles and helps the plasma confine the auxiliary heating. Auxiliary heating of MST with a NBI is dominated by plasma energy confinement times, and is inconsistent with models lacking realistic fast-ion diffusion or that cannot model the entirety of the plasma volume.

ACKNOWLEDGMENTS

[1] M. D. Wyman, B. E. Chapman, J. W. Ahn, A. F. Almagri, J. K. Anderson, F. Bonomo, D. L. Brower, S. K. Combs, D. Craig, D. J. Den Hartog *et al.*, Phys. Plasmas **15**, 010701 (2008).
[2] G. G. Kelley, O. B. Morgan, L. B. Stewart, W. L. Stirling, and H. K. Forsen, Nucl. Fusion **12**, 169 (1972).
[3] L. A. Berry, J. D. Callen, R. J. Colchin, G. G. Kelley, J. F. Lyon, and J. A. Rome, Phys. Rev. Lett. **34**, 1085 (1975).
[4] M. M. Menon, Proc. IEEE **69**, 1012–1029 (1981).
[5] M. Murakami, R. C. Isler, J. F. Lyon, C. E. Bush, L. A. Berry, J. L. Dunlap, and G. R. Dyer, Phys. Rev. Lett. **39**, 615 (1977).
[6] J. S. deGrassie, R. J. Groebner, and K. H. Burrell, Phys. Plasmas **13**, 112507 (2006).
[7] M. Shimada, D. J. Campbell, V. Mukhovatov, M. Fujiwara, N. Kirneva, K. Lackner, M. Nagami, V. D. Pustovitov, N. Uckan, and J. Wesley, Nucl. Fusion **47**, S1 (2007).
[8] J. D. Lawson, CLM-R-171, Culham Laboratory, 1977.
[9] K. A. Werley, Nucl. Fusion **31**, 567 (1991).
[10] K. Hattori, Y. Hirano, Y. Yagi, T. Shimada, and K. Hayase, Fusion Technol. **29**, 1619 (1995).
[11] H. Sakakita, S. Kiyama, Y. Hirano, Y. Yagi, H. Koguchi, T. Shimada, Y. Sato, and K. Hayase, in 30th EPS Conference on Controlled Fusion and Plasma Physics, St. Petersburg, Russia, 7–11 July 2003.
[12] H. Koguchi, H. Sakakita, Y. Hirano, K. Yambe, L. Frassinetti, F. Auriemma, D. Terranova, P. Innocente, S. Kiyama, and T. Shimada, in Proceedings of the 22nd IAEA Fusion Energy Conference EX/P5-25, Geneva, Switzerland, 13–18 October 2008.
[13] G. Fiksel, B. Hudson, D. J. Den Hartog, R. M. Magee, R. O'Connell, S. C. Prager, A. D. Beklemishev, V. I. Davydenko, A. A. Ivanov, and Yu. A. Tsidulko, Phys. Rev. Lett. **95**, 125001 (2005).
[14] G. Fiksel, A. F. Almagri, J. K. Anderson, A. D. Beklemishev, B. E. Chapman, D. Craig, V. I. Davydenko, D. J. Den Hartog, D. Ennis, S. Gangadhara *et al.*, in *Proceedings of the 21st IAEA Conference*, Chengdu, Switzerland, 16–21 October 2006.
[15] B. E. Chapman, A. F. Almagri, J. K. Anderson, T. M. Biewer, P. K. Chattopadhyay, C.-S. Chiang, D. Craig, D. J. Den Hartog, G. Fiksel, C. B. Forest *et al.*, Phys. Plasmas **9**, 2061 (2002).
[16] J. S. Sarff, N. E. Lanier, S. C. Prager, and M. R. Stoneking, Phys. Rev. Lett. **78**, 62 (1997).
[17] D. L. Brower, Y. Jiang, W. X. Ding, S. D. Terry, N. E. Lanier, J. K. Anderson, C. B. Forest, and D. Holly, Rev. Sci. Instrum. **72**, 1077 (2001).
[18] J. A. Reusch, M. T. Borchardt, D. J. Den Hartog, A. F. Falkowski, and D. Holly, Rev. Sci. Instrum. **79**, 10E733 (2008).
[19] J. S. Sarff, A. F. Almagri, J. K. Anderson, T. M. Biewer, A. P. Blair, M. Cengher, B. E. Chapman, P. K. Chattopadhyay, D. Craig, D. J. Den Hartog *et al.*, Nucl. Fusion **43**, 1684 (2003).
[20] T. M. Biewer, C. B. Forest, J. K. Anderson, G. Fiksel, B. Hudson, S. C. Prager, J. S. Sarff, and J. C. Wright, Phys. Rev. Lett. **91**, 045004 (2003).
[21] T. M. Biewer, Ph.D. dissertation, University of Wisconsin-Madison, 2002.
[22] J. Crank and P. Nicolson, Math. Proc. Cambridge Philos. Soc. **43**, 50 (1947).
[23] R. J. Goldston, D. C. McCune, H. H. Towner, S. L. Davis, R. J. Hawryluk, and G. L. Schmidt, J. Comput. Phys. **43**, 61 (1981).
[24] A. Pankin, D. McCune, R. Andre, G. Bateman, and A. Kritz, Comput. Phys. Commun. **159**, 157 (2004).
[25] V. Kotov, D. Reiter, and A. S. Kukushkin, "Numerical study of the ITER divertor plasma with the B2-EIRENE code package," Bericht des Forschungszentrums Jülich Jül-**4257**, November, 2007.
[26] B. Hudson, Ph.D. dissertation, University of Wisconsin-Madison, 2006.